Science Journal of University of Zakho
DOI: https://doi.org/10.25271/sjuoz

Original article

COAGULATION-FLOCCULATION POTENTIAL OF *Achatina achatina* SHELL IN THE REMOVAL OF SUSPENDED SOLIDS FROM PAINT EFFLUENT

Edith C. Unoka [1], Peter M. Eguvbe[2, *], Augustine C. Ogonegbu[3], Jude O. Otedo[3], Joel Okpoghono[4], Uduenevwo F. Evuen[5], Ochuko J. Abeokuta[6], Augustine Uwague[2], and Anthony A. Ogbuta[7]

[1]Department of Industrial Chemistry, Faculty of Science, Dennis Osadebay University, Asaba, Nigeria
[2]Department of Chemistry, Faculty of Science, Southern Delta University, Ozoro, Nigeria.
[3]Department of Chemical Sciences, Faculty of Science, Dennis Osadebay University, Asaba, Nigeria.
[4]Department of Biochemistry, Faculty of Science, Southern Delta University, Ozoro, Nigeria.
[5]Department of Biochemistry and Molecular Biology, Faculty of Science, Dennis Osadebay University, Asaba, Nigeria.
[6]Department of Industrial Chemistry, Faculty of Science, Southern Delta University, Ozoro, Nigeria.
[7]Department of Chemical Sciences, Faculty of Science, University of Africa, Toru-Orua, Bayelsa State, Nigeria.

*Corresponding author email: eguvbepm@dsust.edu.ng (Tel.: +234-8062075109)

Received: 23, May, 2025
Accepted: 17, Aug, 2025
Published: 12, Jan, 2026

ABSTRACT

The sewage from paint is quite turbid and contains a lot of suspended and scattered particles. *Achatina achatina* (AA) shell's ability to coagulate and flocculate and remove suspended particles from paint effluent was considered. The analyses included Fourier Transform Infrared Spectroscopy (FTIR), Scanning Electron Microscope (SEM) and X-ray Diffraction (XRD). Surface area 64.6 m^2/g; ash content 8.2 %; moisture content 11.964 %; bulk density 0.962 g/cm^{-3}; tapped density 1.389 gcm^{-3}; true density 1.667 gcm^{-3}; porosity 42.29 %; pH 7.9; and pH_{zpc} 6.9 are the results of the samples' delineation. Optimum values obtained from varying the operating parameters are: 500mg/L AA, settling time 30 minutes and pH 8. FTIR result indicates that AA has some functional groups. XRD result indicates that AA consists of aragonite, and SEM shows different surface morphologies before and after coag-flocculation, suggesting effective coagulation. Suspended fragments in the paint effluent sample consistently declined with time, pursuant to time evolution of cluster size allotment. Coagulation period ($\tau_{1/2}$) lowest values of 0.05565 seconds and 0.01209 seconds were recorded at 500 mg/L and pH of 8 respectively. This study provided information on animal based coag-flocculation potential which is beneficial for environmental quality management and environmental disputation.

KEYWORDS: Suspended solids, Paint effluent, Coagulation-Flocculation, *Achatina achatina* Shell, Water Pollutio

1. INTRODUCTION

Polluted water is mainly affected by the bulk. The volume of water that is liberated, along with the quantity of polluting material that is released. A small amount of a harmful chemical released from a ship onto the water can have minimal effects. However, when discharged into a lake or stream, where there is a limited supply of clean water to disperse it, the same amount of the same chemical can have a considerably higher impact (Badawi *et al*., 2022). Water is widely used in the paint industry during manufacturing. Large amounts of highly polluting effluents are produced as a result (Samsami *et al*., 2020).

Paint effluent has a high concentration of suspended and dispersed particles and is a highly turbid effluent (Irshad *et al*., 2023). Its release into the environment blocks light, degrades the quality of the receiving stream, and may pose a hazard to marine life, microbes, and the food chain. Additionally, it results in the collapse of the ecological community and significant health hazards. Hence, paint effluent must be treated before being released into the environment (Viktoryová *et al*., 2022). The coagulation-deflocculation method is important in sewage and water treatment because it is easy and low-cost to apply for cleaning and purifying water. Coagulation-deflocculation is a method of destabilizing stable suspended particles in effluent and aggregating them into flocs for easy removal. According to Irfan *et al*. (2017), flocculation is a method by which destabilized molecules group together to form large agglomerates that can be easily separated. This process usually involves gravity settling. Among the inorganic salts used in studies on chemical treatment of water and wastewater are aluminium sulphate, ferric chloride, lanthanum nitrate, and lanthanum chloride. However, employing these salts has disadvantages, such as accelerating Alzheimer's disease and producing substantial amounts of non-biodegradable sludge (Nair *et al.,* 2021). The availability of the coagulant substance for the treatment processes is another factor to consider. As a result, the coagulants should either be industrial waste products or naturally occurring.

There are other commercially available organic synthetic polymer flocculants, such as the better-known polyacrylamide, although they have acute neurotoxic and carcinogenic effects. Water containing chemical monomers and polymer byproducts that have not yet been reacted could provide health hazards (El Mouhri *et al.,* 2021). Because of these limitations, researchers have become interested in the potential of diverse plants and

Access this article online
https://doi.org/10.25271/sjuoz.2026.14.1.1590
Science Journal of University of Zakho
Vol. 14, No. 01, pp. 185–197 January-2026
Printed ISSN 2663-628X;
Electronic ISSN 2663-6298

animals to aggregate (Badawi *et al.,* 2023). Plant-originated inherent coagulants are frequently lethal-free, harmless, and advantageous to the surroundings, according to findings (Kumar *et al.,* 2020; Adetoro and Ojoawo, 2020). However, collecting and preparing plant extracts is a concern because it takes a lot of time and money. Hence, it is important to develop an alternative coagulant to replace traditional curdling in water treatment, to reduce the harmful effects of using mineral coagulants.

It is now important to use organic coagulants made from animals. Since the study focuses on treating paint wastewater, it's necessary to examine the coagulating and deflocculating ability of the *Achatina achatina* shell."

Achatina achatina shells, commonly known as giant African snail shells, are a promising natural coagulant for wastewater treatment (Iloamaeke *et al.,* 2021). They are chosen because they are rich in calcium carbonate, which plays a key role in neutralizing charges and promoting particle settling during water treatment (Nnaji *et al.,* 2023). Using these shells helps reduce dependence on chemical coagulants, which can have harmful environmental impacts. Achatina shells are readily available in many tropical regions, especially as waste from snail consumption, making them a low-cost and sustainable option. Additionally, their use supports waste recycling, helping minimize environmental pollution while providing an eco-friendly alternative for wastewater treatment.

The objectives of this study are to prepare a coagulant from a snail shell sample and determine the physicochemical features, functional groups available in the coagulant, the surface morphology before and after coagulation, flocculation, and crystallinity, the effect of operating parameters (coagulant dosage, settling time, and initial pH), and the kinetic parameters. Snail shells can be used to produce calcium oxide nanoparticles, which have been shown to be effective in treating industrial paint effluent. These nanoparticles can remove heavy metals, organic solvents, and suspended solids from paint wastewater.

2. MATERIALS AND METHODS

Sediment Sampling and Handling:

Snail shell samples were collected from Swali Market, Bayelsa State, Nigeria, and taxonomically identified by a specialist. The effluent sample was obtained from the sewage discharge channel of Hallmark Paint Company located in Onitsha, Nigeria. To eliminate particulate matter and surface impurities, the snail shells were thoroughly washed with deionized water and subsequently air-dried for seven days. The dried shells were then ground into a fine powder and sieved through a mesh with a pore size of 1.9968×10^{-2} cm.

The method described by Adekanmi *et al*. (2023) was employed to process the snail shell powder into a coagulant. Initially, deproteinization was performed by continuously agitating 50 g of the powdered sample in 500 cm^3 of 1 M sodium hydroxide (NaOH) solution at 70°C for two hours. The resulting mixture was filtered and allowed to cool to ambient temperature. The residue was rinsed thoroughly with distilled water for 30 minutes and oven-dried at 70°C for two hours.

Following deproteinization, demineralization was conducted by agitating the dried sample in 250 cm^3 of 1 M hydrochloric acid (HCl) solution for 30 minutes. The mixture was filtered, and the remaining solid residue was rinsed with distilled water for 30 minutes and subsequently dried in a microwave oven at 70°C for two hours.

Finally, deacetylation was performed by treating the demineralized sample with a 50% NaOH solution at a solid-to-liquid ratio of 1:10 (w/v) and agitating for 30 minutes at 121°C. The sample was then rinsed under running water until a neutral pH (pH 7) was achieved, followed by a final rinse with distilled water and microwave drying at 70°C for two hours. The resulting material served as the coagulant used in this study.

Characterization of Specimen:

Exterior area determination:

The ASTM (2015) method was used to calculate the exterior area. The material was acidified to a pH scale of 4 to remove about 0.5g of it. After adding 10 g of dissolved sodium chloride, the volume was brought to 50 mL with distilled H_2O. Titration was performed with 0.1 M NaOH at 298 K until pH 9 was reached using a Lab-tech pH meter. Equation 1 was applied to get the external area and compute the volume required to raise the pH from 4 to 9.

Exterior Area (m^2/g) = 32V – 25 - - - -1

Where V is volume

Ash content assessment:

The ASTM (2015) technique was used to assess the ash capacity. Blank cauldron load was identified as W_1. A pre-measured cauldron was filled with 2 g of the specimen, which was then transported to a muffle furnace and steadily heated up to 550^0C. After heating, the cauldron containing the sample was cooled in a desiccator to room temperature, then tested again. W_2 is the weight of the cauldron with the added ash. Equation 2 was used to evaluate the percentage of ash content.

Percentage Ash Content (%) = $\frac{W_{ash}}{W_{sample}} \times 100$ - - -2

where W_{ash} is the weight of ash = $W_2 - W_1$

W_{sample} is the weight of the specimen

W_1 is the weight of the empty cauldron

W_2 is the weight of the cauldron and ash

Moisture content determination:

The ASTM (2015) technique was used to determine the moisture content. A pre-quantified vessel was packed with 2.0006 g of the specimen, while the load of the blank cauldron was noted as W_1. Following that, this was put on a heater and heated to 105 ^{0}C. The dry specimen was placed inside a cauldron, heated, and then removed. It was weighed again and recorded as W_2. Equation 3 was applied to estimate the moisture potency ratio.

Percentage Moisture Content (%) = $\frac{W_{dry}}{W_{sample}} \times 100$ -3

where W_{sample} is the weight of the specimen before heating

W_{dry} is the weight of the specimen after heating = $W_2 - W_1$

$W_{1\ is}$ the weight of the empty cauldron.

W_2 is the weight of the cauldron and the dry specimen.

Density measurements:

A 100 cm^3 cylinder weighed 25.00 g of sample. Bulk volume (V_{bulk}) was used to represent the volume. The cylinder was repeatedly tapped to maintain a constant volume, which was recorded as Vtapped, the tapped volume. 40 cm^3 of water was placed in an empty cylinder, and the initial volume was recorded. A water-filled cylinder, tapped to a consistent volume known as the true volume V_{true}, received 25.00 g of the sample gradually. Equations 4 to 6 were utilized to evaluate density values.

Bulk density (ρ_{bulk}) = $\frac{M_{sample}}{V_{bulk}}$ - - 4

where M_{sample} is the mass of the specimen

V_{bulk} is bulk volume

Tapped density (ρ_{tapped}) = $\frac{M_{sample}}{V_{tapped}}$ - - -5

where M_{sample} is the mass of the specimen

V_{tapped} is tapped volume

$$\text{True density } (\rho_{true}) = \frac{M_{sample}}{V_{true}} \quad - \quad - \quad 6$$

where M_{sample} is the mass of the specimen
V_{true} is true volume

Porosity:

The porosity was evaluated using equation 7.

$$\text{Porosity} = 1 - \frac{\rho_{tapped}}{\rho_{true}} \quad - \quad 7$$

pH and pH_{zpc} determination:

By adding 100 mL of distilled water to 0.1 g of snail shell sample in a glassware, capping it, and allowing it to acclimate for 2 hours at room temperature, the pH of the sample was determined. A pH meter was used to measure the pH after the sample was left to stand for 24 hours. pH of zero-point charge is known as pH_{zpc}. Using 2 M solutions of NaOH and HCl, the initial pH values of fifteen beakers, each containing 100 cm^3 of 0.1 M sodium chloride solutions, were altered within the ranges of 3-10, varied at 0.5 intervals, for the pHzpc. A Lab-tech pH scale was utilized to evaluate the final pH values of the solutions after 0.1 g of samples were weighed into each of the different beakers and shaken for 24 hours. Plotting $pH_{initial}$ - pH_{final} on the upright axis and $pH_{initial}$ on the abscissa axis yielded values for pH_{zpc}. The pH_{zpc} is assessed by the point of intersection on the $pH_{initial}$ axis.

Analyses of paint effluent:

In line with the benchmark approach for the resolution of H_2O and effluent (APHA, 2017), the biochemical characteristics of the effluent were investigated. pH, temperature, and total suspended solids were the next set of measurements that were analysed.

Coagulation-flocculation Experiments:

Snail shell dosages of 100–500 mg in 200 cm^3 paint effluent were transferred to 300 cm^3 standard flasks. Each flask was exposed to 20 minutes of moderate mixing (30 rpm) after 20 minutes of vigorous mixing (250 rpm) using a magnetic stirrer. The mixture was then put into a glass cylinder and allowed to settle. After 5, 10, 15, 20, 25, and 30 minutes, 50 cm^3 of the supernatant (the top layer of the settling effluent) was pipetted into 100 cm^3 plastic bottles, and the TSS of each supernatant collected at the designated time was determined by filtration. A filter was cleaned, dried, weighed, and then put into the filtering device. The supernatant was stirred, and then 50mL of it was filtered. The filter was cleaned three times after filtering, then placed in an evaporating dish and heated in an oven at 104±1°C for at least 1 hour. The filter was cleared of the kiln after drying and allowed to cool to room temperature in a desiccator. Equation 8 was utilized to rate the TSS for each supernatant (APHA, 2017).

$$\text{Suspended Solids (mg/L)} = \frac{(A-B)\times 1000}{sample(L)} \quad - \quad 8$$

where A is the weight of the filter, and B is the weight of the filter and dry residue.

The ideal AA dosage was established and applied in coag-flocculation studies, with the effluent pH adjusted. Five distinct 300 mL standard flasks, each holding 200 mL of paint effluent, each received 500 mg of snail shell. The pH of each 200 mL paint effluent stored in 300 mL standard flasks was changed to 2, 4, 6, 8, and 10 using 5 M HCl and 5 M NaOH solutions. Each flask was stirred slowly for 20 minutes after being agitated for 2 minutes with a magnetic stirrer, then transferred to a glass cylinder and left to settle. After 5, 10, 15, 20, and 30 minutes, 50 mL of the supernatant was pipetted into 100 mL plastic bottles, and the TSS of each supernatant collected at the designated time was measured.

Fourier Transform Infrared Spectroscopy (FTIR), Scanning Electron Microscopy (SEM), and X-ray diffraction (XRD)

Utilizing Bruker's VERTEX 80v Fourier Transform Infrared Spectroscopy (FTIR) coupled with a digital computer, the functional groups contained in the sample were identified. After being ground to a size below the wavelength of the incident radiation, the samples were smoothed with oil (Nujol). For the purpose of collecting data, the sample was clutched before the beam using IR-transparent salt plates. Before adding another sample, the plate was washed with acetone following each examination.

Using the Carl Zeiss Analytical SEM Series, the sample's surface morphology was characterized. Specimen support was put in the plasma chamber. Later, the specimen to be scanned was mounted on a sample mount in the specimen support. To strike a plasma, the high voltage control was switched on. The high-voltage control was turned off, and the SEM image was acquired after about 1-2 minutes.

The sample's crystallinity was assessed using a PHILIPS X PERT diffractometer and Cu Kr radiation. The data collection was executed using 2^{θ} with a series of 0.00 to 75.00 degrees, the step width of 0.0001, and a step counting time of 29.07 seconds.

Statistical analysis :

ANOVA was used to assess the effects of varying experimental parameters (coag-flocculant dosage, settling time, and effluent pH). The ANOVA was conducted using the Statistical Package for the Social Science (SPSS). This tool is appropriate when there are K groups (K > 2) to improve efficiency while maintaining the type I error rate at the pre-established alpha level.

3. RESULTS AND DISCUSSION :

Physiochemical features:

The results of the physicochemical properties of snail shells are shown in Table 1.

Surface area :

When compared to the surface area value of 40.29 m^2/g for the snail shell determined by Jatto *et al*. 2013, the superficial area value in Table 1 is larger at 64.6 m^2/g. It is assumed that AA will almost certainly do better. The surface area of a coagulant is very important; the more surface area it has, the more coagulation sites it can access. A well-known factor affecting response rate is the average particle size, which is directly linked to the size of the particle pores. According to Al Dubaili and Awad (2012), smaller particles have more surface pores and a greater overall surface area that is accessible to coagulation sites. This fully agrees with the findings of Jiahao et al. (2022), who showed that snail shells are mesoporous. Large surface area usually increases the reaction rate in chemical processes like coagulation-flocculation, and smaller particles provide this larger surface area, as shown by *Achatina achatina*.

Table 1: Physiochemical characterization of *Achatina achatina*.

Parameter	Values
Surface area (m^2/g)	64.6
Ash content (%)	8.2
Moisture content (%)	11.964

Bulk density (g/cm^{-3})	0.962
Tapped density (g/cm^{-3})	1.389
True density (g/cm^{-3})	1.667
Porosity (%)	42.29
Ph	7.70
pH_{zpc}	6.9

Ash content :

For AA, an ash content value of 8.2% was found (Table 1). Obi (2017) recorded a similar number of 5.10%. According to Nguyen *et al*. (2023), AA ash content is a reliable indicator of elemental content and quantifies the portion of inorganic components present. Nhung *et al*. (2023) discovered earlier that the calcium (Ca^{2+}) content of snail shells is particularly high. Calcium (Ca^{2+}) is a crucial component that positively correlates with the surface chemistry of coagulation as to surface charge neutralization. This suggests that snail shells have excellent coagulation capabilities, which are vital in removing suspended particles from aqueous media.

Moisture content :

Comparing the value of 11.964% in Table 1 to the value of 24.33% found for snail shell by Mao *et al*. (2021), the moisture content value is low. The quantity of water that is chemically or physically attached to a substance is identified by its moisture content. It measures the water activity of the area. Moisture content is important because it helps assess a sample's stability and risk of microbial contamination, showing if it can be stored well. Since AA has low moisture content, it is likely to last longer and resist microbial growth (Adekanmi *et al.,* 2023).

Density measurements :

The following are the density values reported in Table 1 : 1.389 g/cm³ (tapped), 1.667 g/cm³ (true), and 0.962 g/cm³ (bulk). The true density of AA surpasses bulk density. Since during actual density measurement the voids containing air are removed. Compared with numbers obtained elsewhere, AA's true density is lower (Ekop *et al*., 2021). The calculated bulk density for AA is 0.962 g/cm³, which is almost equivalent to the 0.67 g/cm³ (CPAC) value that Osabohien *et al*. (2024) reported. Since larger internal surfaces have been demonstrated to improve surface properties of materials with low bulk density, AA offers the excellent surface qualities needed for coagulation.

Particle size, particle size distribution, including particle shape are the main factors that affect the bulk density of powder. According to Baruah and Das, (2021), it is inversely correlated with porosity ; the substance with minor bulk density has higher porosity, and vice versa. For AA, the tapped density equals 1.389 gcm^{-3}. The maximum packing of a powder attained under the influence of clearly defined, externally applied forces is known as the tapped density, which is one of a powder's primary feutres. After forcing a tighter packing of the sample's particles by tapping the container, it provides volume of mass of specimen. Materials are known to become more porous as a result of higher tapping density values (Nnaji *et al*., 2021).

Porosity:

Porosity amount of 42.29 % was determined for AA and the rate is high when compared to the amount of 29.67 % for snail shell reported by Ekop *et al*. (2021) and that of 24.9 % for snail shell reported by Nwajei *et al*. (2024). This means AA has many pores or empty spaces; hence it will likely perform better. Generally, more porous materials have better surface properties. High permeability indicates presence of numerous inward cavities which presents a huge exterior area (Oktaf*et al*. 2023), increasing the availability of the surface charge and consequently better coagulation characteristic.

Paint effluent analyses :

Table 2 displays the findings of the analyses of paint effluent. Due to the kind of primal matter utilized in the paint business, the paint waste has an alkaline pH of 8.65, implying it is acidic. The PE sample's high TSS (1050 mg/L) results are a sign that there are a lot of loose particles are present. The suspended insoluble components present in the waste water are referred to as the total suspended solid. The waste water's measured TSS value was 1050 mg/L, which is significantly higher than the acceptable NESREA level of 100 mgl and indicates that the water was contaminated before treatment. The TSS value dropped to 136.50 mg/L following coag-flocculation treatment with AA, removing 87 % of the hanging insoluble compounds from the wastewater and meeting NESREA standards. This shows that AA was successful in treating the paint waste water.

Table 2 : Paint effluent analyses before and after coagulation

Parameter	Paint Effluent		
	Before	After	NESREA
pH	8.65	7.92	6-9
Temperature (°C)	30	30	25.35
Total Suspended Solid (mg/L)	1050	136.50	100

NESREA National Environmental Standards and Regulations Enforcement Agency

pH and pH_{zpc} determination :

The measured AA pH value of 7.70 indicated a somewhat alkaline property. 6.9 pH_{zpc} was identified as the value. The pH_{zpc} value found is consistent with the 7.9 value published by Nhung *et al*., (2023), however, Diagboya *et al.,* (2023) determined the pH_{zpc} value to be 8.84. pH_{zpc} graph was created using the appendix 7 values for $pH_{initial}$ - pH_{final} versus $pH_{initial}$. pH_{zpc} value for AA, Figure 1 is 6.9, which denotes a nearly neutral characteristic. Given that pH_{zpc} defines the circumstance whereon density of electrical charges on a surface is zero, AA has a surface with zero electrical charges at a pH of 6.9. A closer examination shows that a pH of 6.9 is nearly neutral, indicating that the entire concentration of surface anionic sites is on par with total concentration of surface cationic sites and that negatively and positively charged particles have a fair probability of being attracted to the face of AA (Osabohien *et al*. 2024).

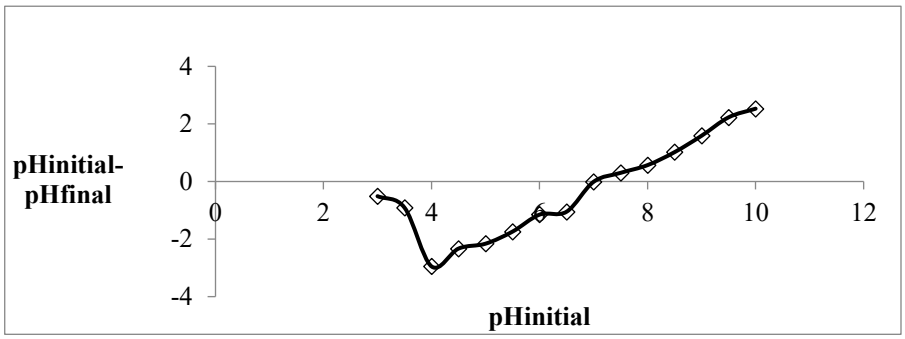

Figure 1: pH_{zpc} for AA

Scanning Electron Microscopy :

Figures 2a and 2b show SEM images of AA before and after coag-flocculation, respectively. Figure 2a reveals that AA has several pores on its exterior. These pores' presence indicates extra surface areas and sticky spots on the AA surface for the effluent particles. On AA (settled floc), destabilized suspended particles may be visible in Figure 2b. On the exterior of the coagulant, aftermath of particle adsorption is observed. The higher particle load on the face of the coagulant is revealed by the more compact structure. Most of the pores were seen to have closed due to particle deposition. Along these lines, Menkiti *et al*. (2016a) and El Mouhri *et al*. (2024) also reported similar results. Figures 2a and 2b demonstrate the potency of AA in the ejection of small particulate from paint manufacturing effluent.

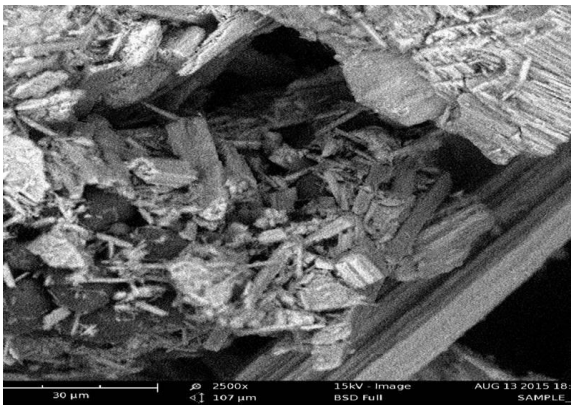

Figure 2a: SEM of AA before Coag-flocculation

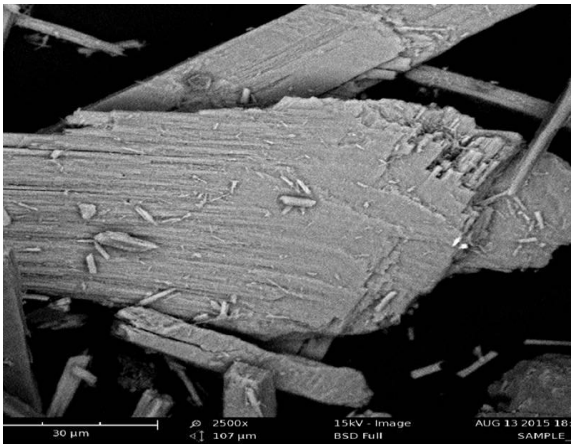

Figure 2b: SEM of AA after Coag-flocculation

X-ray diffraction :

In Figure 3, the X-ray diffraction pattern of AA is seen. Multiple peaks were visible in the XRD pattern of AA, indicating the existence of a transparent phase. A standard JCPDS file was used to identify the crystalline phase. Three significant peaks at 2θ = 18, 24, and 48, which were credited to aragonite (JCPDS: 76-0606), amongst crystal forms of CaCO3, constitute the AA model. The outcome demonstrates that AA contains aragonite. The peak values for aragonite published by Oladoja *et al*. (2011) as well as El Mouhri *et al*. (2024) are quite similar to these.

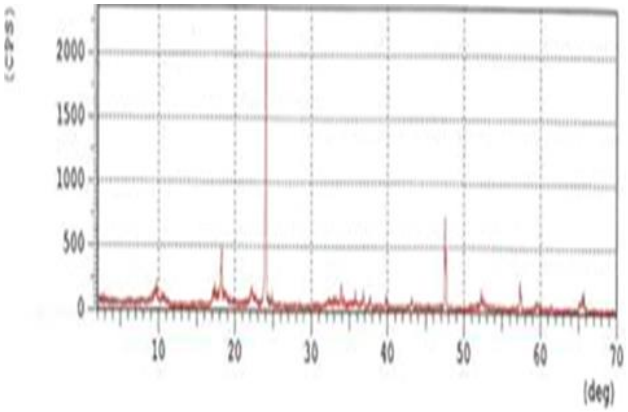

Figure 3: XRD pattern of AA

Fourier Transformed Infrared Spectroscopy (FTIR)

The observed IR peaks from the infrared continuums of AA before and after coagulation are displayed in Table 3. The IR continua of AA before and after coagulation are illustrated in Figures 4a and 4b, respectively. The results were analyzed in conformity with the standard peaks presented by El Mouhri *et al.* (2024) for various functional groups. It is obvious that before coagulation (Fig. 4a), it had more distinct peaks than after coagulation (Fig. 4b). This can be ascribed to the ejection of certain functional groups in the course of the flocculation. Before curdling, distinctive absorption bands appeared at 3734.99cm^{-1}-3523.77cm^{-1}, 1790.27cm^{-1}-1733.03 cm^{-1}, 3502.36cm^{-1}-3177.46 cm^{-1}, 2922.49 cm^{-1}-2853.20 cm^{-1}, 1683.19 cm^{-1}-1635.57cm^{-1}, 860.62 cm^{-1} -712.14 cm^{-1}, which represent amines (N-H), carbonyl (C=O), hydroxyl (O-H), hydrocarbon (C-H), alkene (C=C), and aromatic groups respectively. FTIR continuums of AA after congelation showed distinct peaks at 1788.82cm^{-1}, 3851.21cm^{-1}- 3666.32 cm^{-1}, 2926.14 cm^{-1}, 860.31cm^{-1} -721.73 cm-1, which are characteristic of carbonyl (C=O), amines (N-H), hydrocarbons (C-H), and aromatic groups, respectively. These peak values are in close concord with values reported by Osabohien *et al*. (2024) and El Mouhri *et al*. (2024). The results show that the peaks for alkene and hydroxyl functional groups, which were present in AA before coagulation, were no longer present after the coagulation. This shows that they have been removed in the course of the coagulation.

Table 3 : Observed IR Peaks from the IR spectra of AA before and after coagulation

Before Coag-flocculation		After Coag-flocculation	
IR Peaks (cm^{-1})	Functional Group	IR Peaks (cm^{-1})	Functional Group
3734.99-3523.77	N-H	3851.21- 3666.62	N-H
1790.27-1733.03	C=O	1788.82	C=O
3502.36-3177.46	OH	2926.14	C-H
2922.49-2853.20	C-H	860.31-721.73	Aromatic
1683.19-1635.57 860.62-712.14	C=C Aromatic		

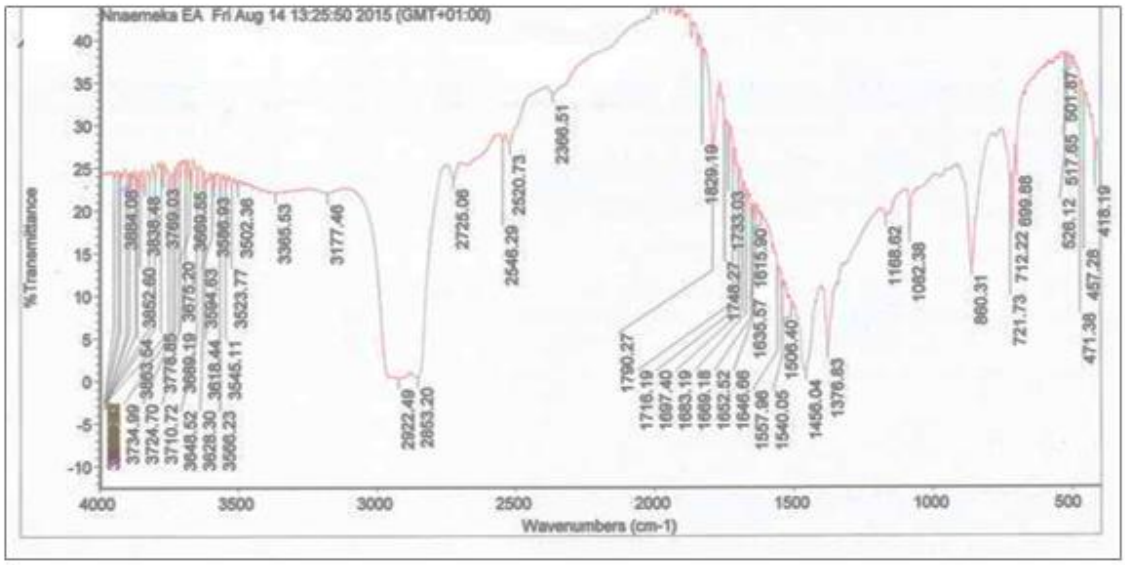

Figure 4a: FT-IR spectraof AA before coag-flocculation

Coag-flocculation: effects of parameter

Impact of coagulant concentration on TSS removal

Table 4 displays the TSS in PE sample findings at varied AA doses and settling times. According to the observable model, the TSS concentration decreased from its starting value of 1050 mg/L to lower values. As the settling moment and AA composition increased, the TSS value declined horizontally and vertically across the table. The certainty that turbidity decreased as settling time increased shows that, from 0 to 30 minutes, there were fewer fragments accessible for coagulation, presumably due to a charge neutralization mechanism as solubilization advanced.

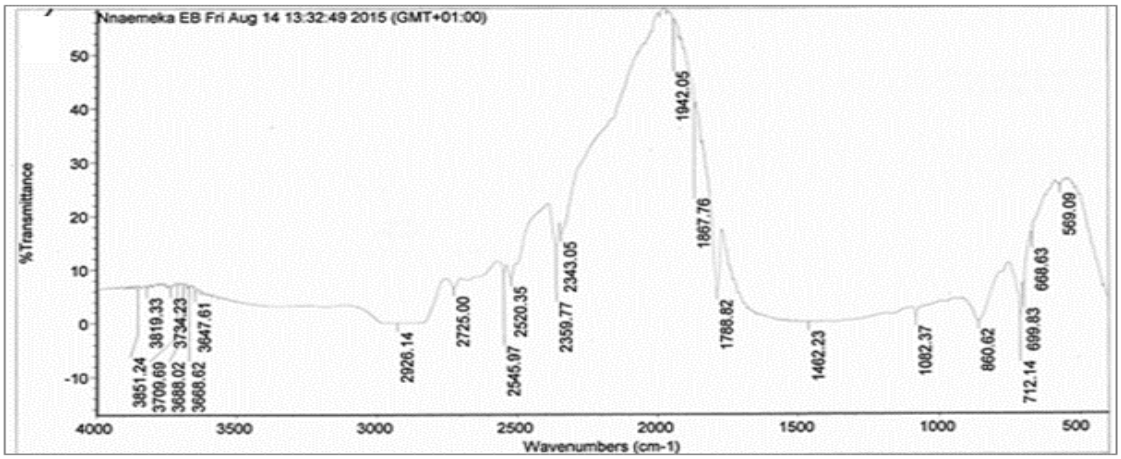

Figure 4b : FT-IR spectraof AA after coag-flocculation

Table 4 demonstrated that the optimal AA dosage is 500 mg/L, suggesting that an increase in the coagulant's surface charge enhances TSS removal from paint industry effluent. Charge neutralization probable reason why AA is effective at removing TSS. The surface charges of the chemical species in AA are attracted to suspended particles at one or more locations, lowering the surface potential and making the suspended solids unstable and prone to forming flocs. Sun *et al*. (2020) noted a comparable tendency.

Table 4: TSS values at various AA dosages and settling time

AA Dosages	TSS values (in mg/L) after different settling times					
	0(mins)	**5(mins)**	**10(mins)**	**15(mins)**	**20(mins)**	**30(mins)**
100 mg/L	1050	542.2	478.8	446.9	425.8	415.2
200 mg/L	1050	525.0	472.5	452.6	430.6	410.6
300 mg/L	1050	430.5	367.5	346.5	326.6	322.3
400 mg/L	1050	388.5	314.8	294.6	285.8	283.2
500 mg/L	1050	336.0	279.3	272.2	260.8	254.3

Table 5 shows the outcome of equation 3 calculation of potency of coag-flocculation in various AA dosages in paint effluent at varied settling times. According to the findings in Table 5, the efficacy of coagulation rose as AA and settling time increased. The ability of the coagulation is a measure of how well the AA coagulant removes TSS. The highest effective dose of AA for removing TSS from paint effluent was 500 mg/L after thirty minutes of settling, whereas the least effective dose was 100 mg/L after five minutes. This is similar with the finding from Miyah *et al*. (2020). In addition, as the AA surface area increased, the AA face charge density of the AA also increased. This suggests that the particles destabilize quickly, presumably through electrostatic synergy with TSS surface, leading to fast coagulation of suspended particles. Figure 5 shows a plot of coagulation-flocculation efficiency over time for different AA dosages in paint effluent (PE) at pH of 8.

Table 5: Efficiency of coag-flocculation with time for varying AA dosages in paint effluent

	Efficiency (in %) at different settling time					
AA Dosages	**0(mins)**	**5(mins)**	**10(mins)**	**15(mins)**	**20(mins)**	**30(mins)**
100 mg/L	1050	48	54	57	59	60
200 mg/L	1050	50	55	57	59	61
300 mg/L	1050	59	65	67	68	69
400 mg/L	1050	63	70	71	72	73
500 mg/L	1050	68	73	74	75	87

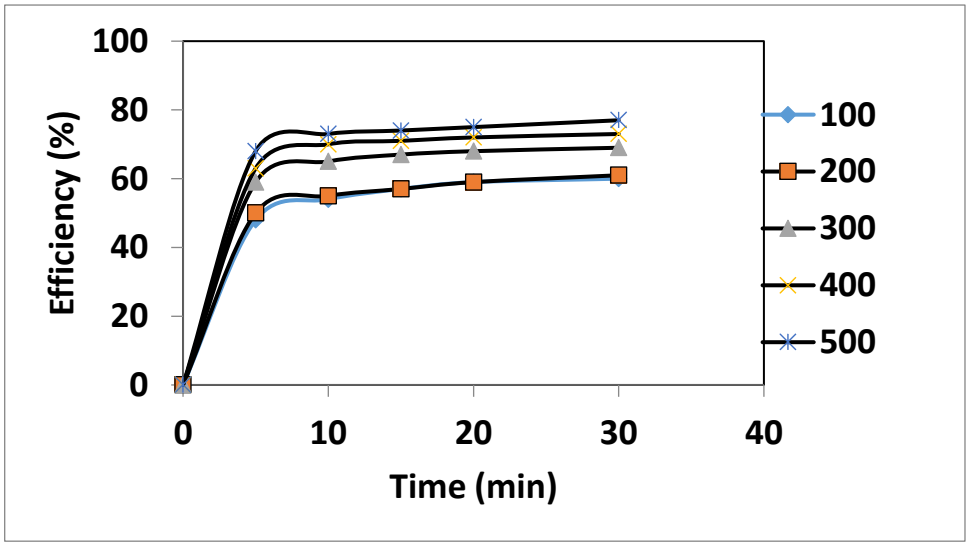

Figure 5: Coag-flocculation performance of different AA dosages at pH

Impact of pH variation on TSS ejection :

Table 6 presents the results for TSS in a PE sample across varying pH levels and settling times. According to the findings in Table 6, TSS reduction was noticeable at all pH levels investigated, with the best turbidity removal happening at a pH of 8 after 30 minutes of settling. Positively charged particles indicate that double-layer compression, an inadequate coagulation mechanism, perhaps the cause of the observed lower efficiency in TSS removal at acidic effluent pH levels (Appiah-Brempong, 2023). The solution's ionic strength may have grown as a result of the acid's positively charged ions, that may have compressed the electric dual layer which causes electrostatic repulsion.

Table 6: TSS values at varying pH and settling time

pH	TSS values (in mg/L) at different settling time					
	0(mins)	5(mins)	10(mins)	15(mins)	20(mins)	30(mins)
2	1050	525	472.5	441	399	367.5
4	1050	483	441	441	420	346.5
6	1050	430.5	367.5	336	294	262.5
8	1050	304.5	262.5	231	210	136.5
10	1050	409.5	346.5	325.5	294	273

A large concentration of hydroxides, carbonates, or bicarbonates at pH levels higher than 8 causes the surface charge on the AA coagulant to become more negative. At pH levels higher than 8, charge annulment and linking mechanisms may be enmeshed in the ejection of TSS from paint industry effluent. It's likely that certain of the AA coagulant's chemical group adsorbed at the suspended solid's surface to build a bridge that connects to numerous additional suspended solids and causes floc to form. This concurs with the research conducted by Sun *et al*. (2019). Outcome of equation 3's calculation of the AA coagulation efficiency over time and at various pH levels in paint effluent are displayed in Table 7

Table 7 : Efficiency of coag-flocculation with time at various pH in paint effluent

pH	Efficiency (in %) at different settling time					
	0(mins)	5(mins)	10(mins)	15(mins)	20(mins)	30(mins)
2	1050	50	55	58	62	65
4	1050	54	58	58	60	67
6	1050	59	65	68	72	75
8	1050	71	75	78	80	87
10	1050	61	67	69	72	74

The results in Table 7 demonstrate that as pH and soothing time increased, the coagulation capability increased as well. The capacity of 87% at pH 8 is the optimal pH for peak TSS elimination. After 5 minutes, pH 2 had the lowest TSS discharge capacity, which was 50%. This suggests that a slightly alkaline medium is more suited for TSS removal through charge neutralization and interparticle bridging. Sun *et al*. (2019) reported a similar outcome. Roy *et al*. (2023) reported that tannin coagulant had an acidic pH. Figure 6 shows a graph of coag-flocculation efficiency with time for different pH in paint effluent (PE) at a dosage of 500 mg/L AA. A close examination of Figure 6 reveals that the requirements for these trials were best met and the topmost investigated AA dosage in a medium that was slightly alkaline.

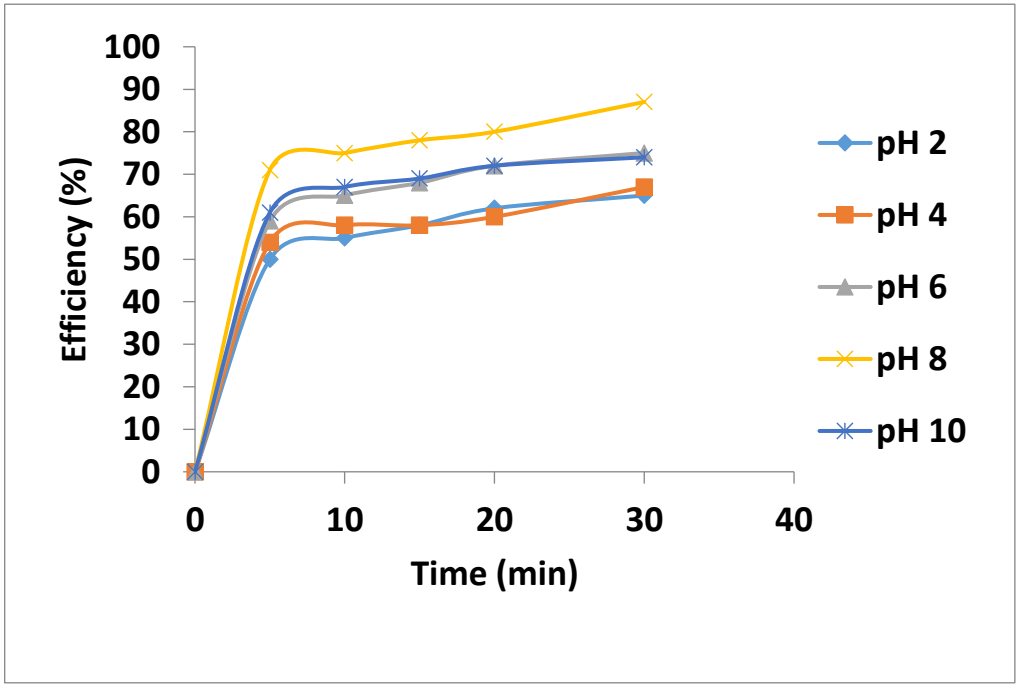

Figure 6: Coag-flocculation performance of 500 mg/L AA dosage at different pH values

Analysis of variance (ANOVA)

Table 8 displays the ANOVA for the influence of coag-flocculant dosage on AA's coagulation performance. ANOVA was used to determine whether there were any significant differences between the coagulation capacity values in appendix 9 obtained for AA in various paint effluent pH and AA dosages at various settling durations. TSS removal from paint industry waste water is significantly influenced by coagulant dosage, settling period, and sewage starting pH, according to values of significance less than 0.05. The estimated mean square values for the initial pH of the sewage, the recommended dose of AA, and the balancing time are 362.706, 314.488, and 221.342, apart.

Table 8: ANOVA for coag-flocculant dosage effect on coagulation performance of AA.

Source of Variance	Sum of Squares	Df	Mean Square	F_{cal}	Significance
Dosage	1257.951	4	314.488	73.359	0.000
pH	1450.824	4	362.706	84.606	0.000
Time	885.369	4	221.342	51.631	0.000
Error	158.619	37	4.287		
Total	3752.763	49			

The highest mean square value is found in paint effluent pH, indicating that AA dosage, restful time, and pH have the greatest effects on TSS elimination. Elemike *et al*. (2017) had earlier reached a similar finding. Musteret *et al*. (2021) previously reported on the statistical differences of parameter effects for TSS removal using ANOVA. ANOVA is increasingly useful for determining whether the studied parameters differ significantly across the examined factors.

Coag-flocculation kinetics studies :

The kinetic plots obtained from equations 9 and 10 are shown in Figures 7 –10.

$$\ln N = -k_R t + \ln N_o \quad - \quad - \quad 9$$

Where k_R represents the reaction rate constant, No and N are the initial concentration and the concentration at time t, respectively. For first-order reaction kinetics, the graph of ln N as a function of time should give a straight line graph with a slope k_R and an intercept of ln N_o.

$$\frac{1}{N} = \frac{1}{N_o} + k_R t \quad - \quad - \quad -10$$

Where k_R is the reaction rate constant, N_o and N are the initial concentration and concentration at any time t, respectively. For second order coagulation kinetics, a graph of 1/N versus time should yield a linear graph with a gradient of k_R and intercept of $1/N_o$.

Figures 7 through 10 displayed that the 500 mg/L AA dosage, which had the maximum surface area and surface charge density and pH 8 correspondingly, had the highest coagulation rate for TSS elimination. Tables 9 for various AA doses and Table 10 for various paint effluent pH exhibit the dynamic characteristics determined from the first order and 2nd order kinetic models. The slope (kR) values listed in Tables 9 and 10 showed very little variation. The second order kinetic model produced a maximum kR value at a coagulant dosage of 500 mg/L and pH 8. Since the neutralization rate of the surface charge of the suspended particles is optimal subject to these terms, a higher coagulation rate is anticipated.

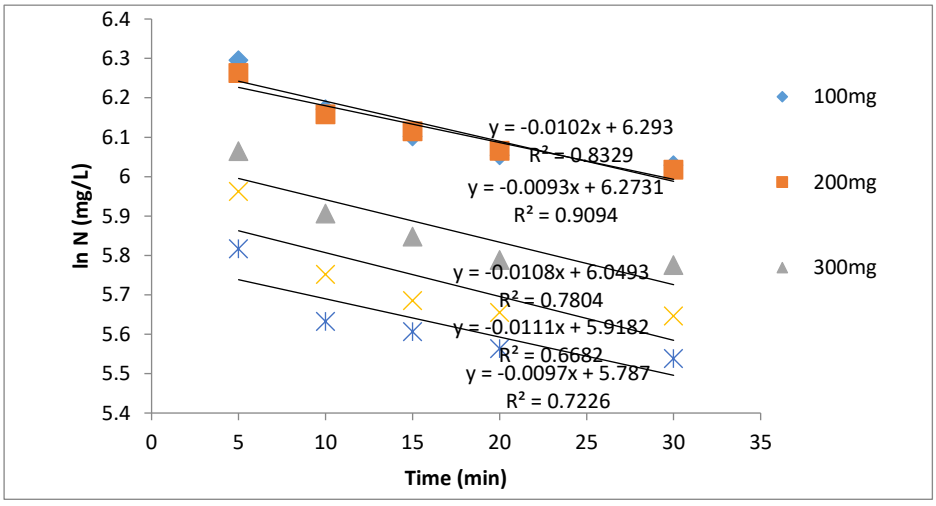

Figure 7: First order plots for different AA dosages in paint effluent at pH 8.

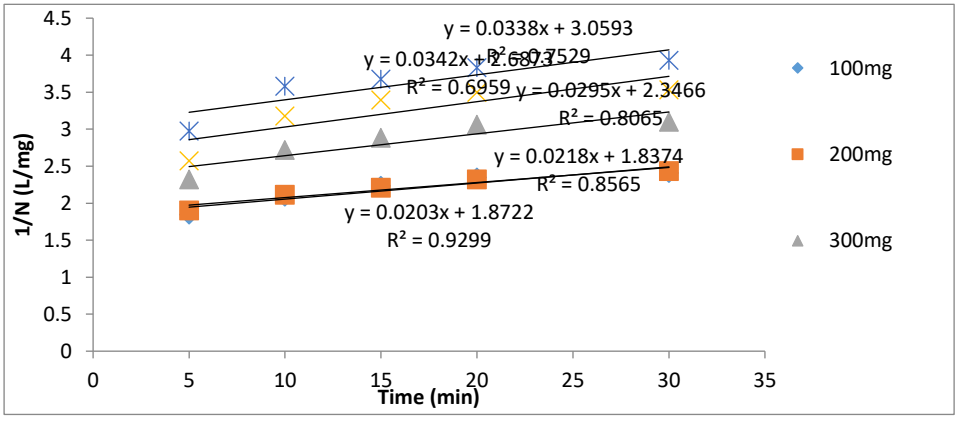

Figure 8: Second-order plots for different AA dosages in paint effluent at pH 8

A measure of the intensity with which particles vanish during a coagulation-flocculation process, kR is essentially the rate per unit particle concentration. A fast rate of aggregation is reliant on a short coagulation time (τ1/2). The lowest values of τ1/2 from the second-order kinetic model were found at 500mg/L and pH 8 in Tables 9 and 10. This matches the outcome found by Obi (2017).

To determine if the test findings were compatible with the kinetic model represented by equations 9 and 10, the linear regression coefficient (R^2) was used. Regarding the findings in Tables 9 and 10, the first-order kinetic model yielded R2 values between 0.6882 and 0.9773, whereas the second-order kinetic model yielded values between 0.6959 and 0.9818. These findings imply that the first-order and second-order kinetic models were followed during the AA-induced coagulation therapy of PE. R^2 values are in the ballpark of those reported in earlier studies by Diagboya *et al*. (2023).

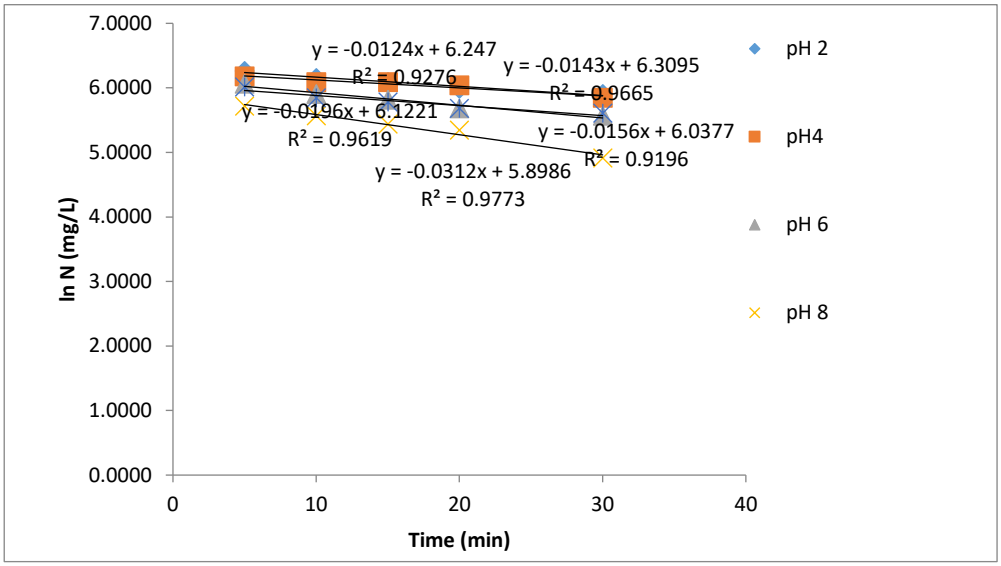

Figure 9: First order plots for different pH in paint effluent at 500mg/L.

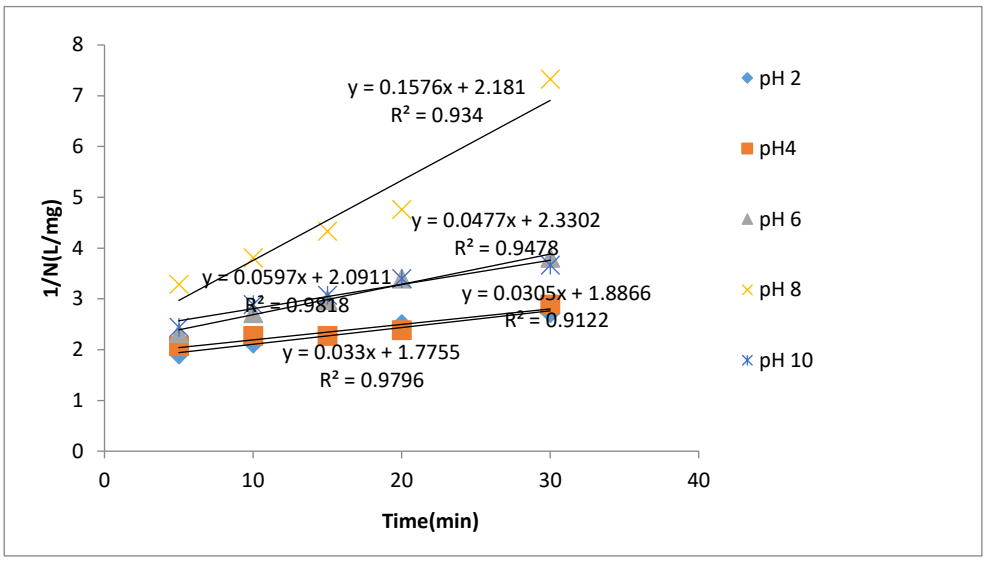

Figure 10: Second-order plots for different pH in paint effluent at 500mg/L

Test results are best fit by the second-order kinetic model because its R^2 values were higher (more closely related to unity) in general comparison to the first order and second order reaction kinetics functional parameters. Related findings were gotten by Osabohien *et al.* (2024).

Time Evolution of the Cluster Size Distribution :

$$N_1 = 4N_0 (2+ k_R N_0 t)^{-2} \quad - \quad - \quad 11$$

$$N_2 = 4N_0^2 k_R t(2+ k_{sl} N_0 t)^{-3} \quad - \quad - \quad 12$$

$$N_3 = 4N_0^3(k_R t)^2 (2+ k_R N_0 t)^{-4} \quad - \quad 13$$

A general representation of equations 11, 12, and 13 can be expressed thus

$$N_m(t) = 4N_0^m(k_R t)^{m-1} (2+ k_R N_0 t)^{-(m+1)} \quad - \quad - \quad 14$$

Table 9: Kinetic parameters for different AA dosages

Model	Dosage (mg)	Parameters			
		k_R(L/mg.min)	R^2	$\tau_{1/2}$(s)	Rate Equation (mg/l.min)
First order	100	0.01017	0.8329	0.1873	-0.010165x + 6.292962
	200	0.009334	0.9094	0.2041	-0.009334x + 6.273116
	300	0.01078	0.7804	0.1767	-0.010784x + 6.049265
	400	0.009707	0.7226	0.1962	-0.009707x + 5.786957
	500	0.01112	0.6682	0.1713	-0.011124x + 5.918216
Second order	100	0.02176	0.8565	0.08754	0.021764x + 1.837384
	200	0.02035	0.9299	0.0936	0.020346x + 1.872216
	300	0.02952	0.8065	0.06452	0.029523x + 2.346632
	400	0.03376	0.7529	0.05642	0.033758x + 3.059270
	500	0.03423	0.6959	0.05564	0.034229x + 2.687297

Table 10: Kinetic parameters for different paint effluent pH

Model	pH	Parameters			
		k_R(L/mg.min)	R^2	$\tau_{1/2}$(sec)	Rate Equation (mg/l.min)
First order	2	0.01427	0.9665	0.1335	-0.014272x + 6.309470
	4	0.01236	0.9276	0.1541	-0.012358x + 6.246954
	6	0.01960	0.9619	0.09718	-0.019601x + 6.122122
	8	0.03123	0.9773	0.06099	-0.031225x + 5.898562
	10	0.01559	0.9196	0.1222	-0.015586x + 6.037684
Second order	2	0.03298	0.9796	0.05776	0.032981x + 1.775503
	4	0.03049	0.9122	0.06247	0.030488x + 1.886646
	6	0.05969	0.9818	0.03191	0.059691x + 2.091127
	8	0.1576	0.9340	0.01209	0.157569x + 2.180997
	10	0.04767	0.9478	0.03996	0.047669x + 2.330222

For Forms 1, 2, and 3, respectively, the time evolution of aggregating particles, monomers, dimmers, and trimmers was predicted using equations 11, 12, and 13. The numbers from Equations 11, 12, and 13 in the annexes were utilized to produce the graph in Figures 11–20 for the trends of the aggregating particles as a function of time. Figures 11–20 illustrate how the suspended matter in paint effluent decreased and gathered on the coagulant's surface. The overlap of the plots for monomers, dimmers, and trimmers in the paint effluent decreased quickly and uniformly. In each plot, the elimination of particles showed a consistent pattern. This is so that dimers and trimmers, which hasten the curdling process by rapidly destabilizing monomers, can develop.

The sum, which is an indication of the decline in the total number of particles (∑N) from the paint effluent, their adsorption, and distribution on the face of the AA coagulant, was created by the monomers, dimmers, and trimmers. All of them demonstrate how well equation 14 fits the particle size distribution and agrees with other studies of coag-flocculation (Chen *et al.* 2024).

CONCLUSION

This study investigated the use of *Achatina achatina* shell-based coagulant for treating paint effluent (PE). Experimental analysis showed that increasing the coagulant dosage, using a pH of 8, and extending the settling time enhanced the coagulation process. Kinetic modeling revealed that the reaction followed a second-order rate model for both coagulation and flocculation. Instrumental analyses using FTIR and SEM confirmed that AA possesses strong coagulation properties. The highest removal efficiency of 87% was achieved at an optimal AA dosage of 500 mg/L, pH 8, 30 minutes settling time, and 30°C, reducing the total suspended solids (TSS) from 1050 mg/L to 136.5 mg/L. Over time, suspended particles in the effluent steadily decreased, aligning with changes in particle size distribution. Overall, the findings demonstrate that AA is an effective natural coagulant for treating paint effluent using the coag-flocculation method.

Acknowledgment

The authors gratefully acknowledge the Department of Chemistry, Faculty of Science, Southern Delta University, Ozoro, for their support and for providing the necessary facilities to conduct this research.

Author Contribution:

Conceptualization, E.C.U., P.M.E., and A.C.O.; methodology, J.O.O. and J.O.; software, U.F.E.; validation, O.J.A., A.U., and A.A.O.; formal analysis, E.C.U. and P.M.E.; investigation, J.O.O., J.O., and U.F.E.; resources, O.J.A. and A.U.; data curation, A.A.O.; writing original draft preparation, E.C.U., P.M.E., and A.C.O.; writing review and editing, J.O.O., J.O., U.F.E., and O.J.A.; visualization, A.U.; supervision, A.C.O. and A.A.O.; project administration, E.C.U.; funding acquisition, P.M.E. All authors have read and agreed to the published version of the manuscript.

Ethical statement:

The Ethical Committee of the Southern Delta University, Ozoro, Nigeria (SDU Ethical Code: 023; 2024), approved the current experiment.

REFERENCES

Ardila, J., Bijker, W., Tolpekin, V., & Stein, A. (2012). *Gaussian localized active contours for multitemporal analysis of urban tree crowns*. Paper presented at the 2012 IEEE International Geoscience and Remote Sensing Symposium. DOI: 10.1109/IGARSS.2011.6049856

Adekanmi A. A., Adekanmi U. T., Adekanmi A. S., Ahmad L. K. and Emmanuel O. O. (2023) Production and characterization of chitosan from chitin of snail shells by

sequential modification process, Afric. J. Biotechnol., 22(2), 39-53, https://doi.org/10.5897/AJB2020.17135.

Adetoro E. A., and Ojoawo S. O. (2020) Optimization study of biosorption of toxic metals from mining wastewater using Azadirachta indica bark adsorbents, Wat. Sci. Technol., 82(5), 887–904, https://doi.org/10.2166/wst.2020.394

Al Dujaili A. H., and Awwad A. M. (2012) Biosorption of cadmium (II) onto loquat leaves (Eriobotrya japonica) and their ash from aqueous solution, equilibrium kinetics, and thermodynamic studies, Internat. J. Industr. Chem., 3(22), 1-7, https://doi.org/10.1186/2228-5547-3-22

APHA/AWWA/WEF (2017) Standard methods for the examination of water and wastewater, 23rd edn. American Public Health Association, American Water Works Association, Water Environment Federation, Denver, p 874.

Appiah-brempong M., Michelle H., Essandoh K., Asiedu N. Y., Dadzie S. K., and Momade F. Y. (2023) Performance optimization of chemical and green coagulants in tannery wastewater treatment: A response surface methodology approach, J. Optimiza., 19, https://doi.org/10.1155/2023/9939499

ASTM D629-15 (2015) American Society for Testing and Materials, ASTM International, West Conshohocken, PA.

Badawi A. K., Ismail B., Baaloudj O., and Abdalla K. Z. (2022) Advanced wastewater treatment process using algal photo-bioreactor associated with dissolved air flotation system: A pilot-scale demonstration, J. Wat. Proc. Engin., 46, 102565, https://doi.org/10.1016/j.jwpe.2022.102565

Badawi A. K., Salama R. S., and Mostafa M. M. (2023) Natural-based coagulants/flocculants as sustainable market-valued products for industrial wastewater treatment: A review of recent development, Roy. Soc. Chem. Advan., 13, 19335-19355, https://doi.org/10.1039/d3ra01999crsc.li/rsc-advances

Baruah B. K., and Das B. (2021) Assessment of soil fertility status for sustainable productivity: A study in some tea garden belts of Assam, India. Curr. Perspect. Chem. Sci., 6, 128-141, https://dx.doi.org/10.9734/bpi/cpcs/v6

Chen G., Gallegos M. J., Soetrisno D. D., Vekilov P. G., and Conrad, J. C. (2024) A minimal colloid model of solution crystallization nucleates crystals classically, Soft. Matt., 20(11), 2575-2583, https://doi.org/10.1039/D35M01609A

Diagboya P. N., Heyde B. J., and Düring R. A. (2023) Efficient decontamination of aqueous glyphosate using Santa Barbara Amorphous-15 (SBA-15) and graphene oxide-SBA-15 poly-amidoamine functionalized composites, Chemic. Engineer. J., 143263, https://doi.org/10.1016/j.cej.2023.143263

Ekop I. E., Simontan K. J., and Onwuka U. N. (2021) Comparative analysis of physical properties of two varieties of periwinkle relevant to the design of processing equipment, Res. Agricultur. Engineer., 67, 45–50, https://doi.org/10.17221/58/2020-RAE

Elemike E. E., Onwudiwe D. C., Ekennia A. C., Ehiri R. C., and Nnaji N. J. (2017) Phytosynthesis of Silver Nanoparticles using Aqueous Leaf Extracts of Lippia Citriodora: Antimicrobial, Larvicidal and Photocatalytic Evaluations, Mater. Sci. Engineer., 75, 980–989, https://doi.org/10.1016/j.msec.2017.02.161

El mouhri G., Merzouki M., Kachkoul R., Belhassan H., Miyah Y., Amakdouf H., Elmountassir R., and Lahrichi A. (2021) Fixed-bed adsorption of tannery wastewater pollutants using bottom ash: an optimized process, Surfac. Interfac., 22, https://doi.org/10.1016/j.surfin.2020.100868

El Mouhri G., Elmansouri I., Amakdouf H., Belhassan H., Kachkoul R., El oumari F. E., Merzouki M. and Lahrichi A. (2024) Evaluating the effectiveness of coagulation–flocculation treatment on a wastewater from the moroccan leather tanning industry: An ecological approach, Heliyon, 10, e27056, https://doi.org/10.1016/j.heliyon.2024.e27056

Iloamaeke I. M., Nnaji N. J., Okpala E. C., Eboatu A. N., and Onuegbu T. U. (2021) *Mercenaria mercenaria* shell: Coagulation-flocculation studies on colour removal by response surface methodology and nephlometric kinetics of an industrial effluent. Journal of Environmental Chemical Engineering, 9(4). https://doi.org/10.1016/j.jece.2021.105715

Irfan M., Butt T., Imtiaz N., Abbas N., Khan R. A., and Shafique A. (2017) The removal of COD, TSS and colour of black liquor by coagulation–flocculation process at optimized pH, settling and dosing rate, Arab. J. Chem., 10(S2), S2307-S2318, https://doi.org/10.1016/j.arabjc.2013.08.007

Irshad M. A., Ali B., Irfan A., Al-Hussain S. A., Nawaz R., Nasim I., Latif M., and Zaki M. E. A. (2023) Sustainable and safe treatment of wastewater of paint industry using Azadarachta indica leaf extract combined with silver nitrate solution, Sustainability, 15, 3592, https://doi.org/10.3390/su15043592

Jiahao A., Nguyen T. N., Yaxuan D., Hao C. (2022). Chestnut shell-activated carbon mixed with pyrolytic snail shells for methylene blue adsorption, Materials. 15, 8227, https://doi.org/10.3390/ma15228227

Kumar A., Singh E., Khapre A., Bordoloi N., Kumar S. (2020) Sorption of volatile organic compounds on non-activated biochar, Bioresourc. Technol., 297, 122469, https://doi.org/10.1016/j.biortech.2019.122469

Mao S., Xu X., Zhang L., Bai B., Hu N. Wang H. (2021) Methylated mud snail protein as a bio-flocculant for high turbidity wastewater treatment, Wat. Sci. Technol., 84(3), 737, https://doi.org/10.1016/j.biortech.2019.122469

Menkiti M. C., Ezemagu M., Okolo B. (2016a) Perikinetics and sludge study for the decontamination of petroleum produced water using Novel Mucuna Seed Extract, Petrol. Sci., 13, 328–339, https://doi.org/10.1007/s12182-016-0082-9

Miyah Y., Lahrichi A., Kachkoul R., El Mouhri G., Idrissi M., Iaich S., Zerrouq F. (2020) Multi-parametric filtration effect of the dyes mixture removal with the low cost materials, Arab. J. Bas. Appl. Sci., 27, 248–258, https://doi.org/10.1080/25765299.2020.1776008

Mustereț C. P., Morosanu I., Ciobanu R., Plavan O., Gherghel A., Al-Refai M., Roman I., Teodosiu C. (2021) Assessment of coagulation–flocculation process efficiency for the natural organic matter removal in drinking water treatment, Wat. (Switzerland)., 13, https://doi.org/10.3390/w13213073

Nair S., Manu B., Azhoni A. (2021) Sustainable treatment of paint industry wastewater: Current techniques and challenges, J. Environ. Managt.,296, 113105, https://doi.org/10.1016/j.jenvman.2021.113105

Nguyen T. H. N., Vo D. L., Toyohisa F. (2023) A critical review of snail shell material modification for applications in wastewater treatment, Mater. (Basel)., 16(3), 1095, https://doi.org/10.3390%2Fma16031095

Nhung N. T. H., Long V. D., Fujita T. (2023) A critical review of snail shell material modification for applications in wastewater treatment, Mater. (Basel, Switzerland)., 16(3), 1095, https://doi.org/10.3390/ma16031095

Nnaji N. J., Okafor N. I., Ekwonu A. M., Osuji O. U., Okwukogu O. O., Okoye O., Anozie A. I., Anene S. C., Ehiri R. C., Onuegbu T. U. (2021) Cashew nut testa tannin resin –

preparation, characterization and adsorption studies, J. Taibah. Uni. Sci., 15:1, 170-183. https://doi.org/10.1080/16583655.2021.1930717

Nnaji N. J., Sonde C. U., Nwaji O. L., Ezeh G. C., Onuigbo A. U., Ojukwu A. M., Mbah P. C., Adewumi A. O., Unoka E. C., Otedo J. O., and Onuegbu T. U. (2023). *Dacryodes edulis* leaf derived biochar for methylene blue biosorption. Journal of Environmenal Chemical Engineering, 11(3). https://doi.org/10.1016/j.jece.2023.1096

Nwajei B. A., Jacob J. N., and Okuo J. M. (2024) Comparative studies on the use of activated snail (Achanita fulica) and perewinkle shells (Typanotonous fuscatu) in the removal of heavy metal ions from aqueous solutions. Ife. J. Sci., 25(3), 331-343. https://dx.doi.org/10.4314/ijs.v25i3.1

Obi C. (2017). Application of Coagulation and Electro-coagulation in Abattoir Wastewater Treatment, M.Sc Thesis, Nnamdi Azikiwe University, Awka, Nigeria.

Oktaf R., Anggi S., Yatim R. W., Syahdilla A. A. R., Ajis P., and Aang H. (2023). Characteristic physicochemical of bamboo-based activated carbon for coal run-off water treatment used at Pt.bukit Asam sludge settlement pond, Internat. J. Soc. Sci., 3(1), 91–96, https://doi.org/10.53625/ijss.v3i1.6380

Oladoja N. A., Raji I. O., Olaseni S. E. & Onimisi T. D. (2011). In-situ hybridization of waste dyes into growing particles of calcium derivatives synthesized from a gastropod shell (Achatina achatina), Chemi. Engineer. J., 171, 941– 950, https://doi.org/10.1016/J.CEJ.2011.04.044

Osabohien E., Overah L. C., Anikwushe Y. U. & Eguvbe P. M. (2024) Comparative Pb(II) Adsorption by Activated Carbon from African Star Apple (Chrysophylum albidum) and Pawpaw (Carica papaya) Seeds, Nig. J. Sci. Environ., 22(1), 161–179, https://doi.org/10.61448/njse2212413

Roy K., Dey T. K., Zuha S. T., Jamal M., Srivastava M., and Uddin M. E. (2023). Removal of turbidity from tannery wastewater using graphene oxide-ferric oxide nanocomposites as an adsorbent, Int. J. Environ. Sci. Technol., 20, 5597–5608, https://doi.org/10.1007/s13762-022-04301-w

Samsami S., Mohamadi M., Sarrafzadeh M. H., Rene E. R., and Firoozbahr M. (2020). Recent advances in the treatment of dye-containing wastewater from textile industries: Overview and perspectives, Proc. Safet. Environ. Protect., 143, 138–163, doi:10.1016/j.psep.2020.05.034

Sun H., Jiao R., Xu H., An G., and Wang D. (2019). The influence of particle size and concentration combined with pH on coagulation mechanisms, J. Environ. Sci., 82, 39–46, https://doi.org/10.1016/j.jes.2019.02.021

Sun Y., Zhou S., Sun W., Zhu S. & Zheng H. (2020). Flocculation activity and evaluation of chitosan-based flocculant CMCTS-g-P(AM-CA) for heavy metal removal, Separa. Purific. Technol., 241, 116737, https://doi.org/10.1016/j.seppur.2020.116737

Viktoryová N., Szarka A., and Hrouzková S. (2022) Recent developments and emerging trends in paint industry wastewater treatment methods, Appl. Sci.,12, 10678, https://doi.org/10.3390/app122010678